集会　2013 年 11 月 8 日　松本

27. 工藤 幸司、岡村 信行、古本 祥三、原田 龍一、古川 勝敏、樋口 真人、Victor L Villemagne、谷内 一彦、荒井啓行: タウイメージング用 PET プローブの現状. 第 32 回日本認知症学会学術集会　ホットトピック　2013 年 11 月 8 日～10 日　松本
28. 岡村信行、古本祥三、原田龍一、多胡哲郎、岩田錬、谷内一彦、工藤幸司、Michelle T Fodero-Tavoletti、Christopher C Rowe 、 Victor L. Villemagne . [^{18}F]THK-5105 を用いたアルツハイマー病脳内タウ蛋白の PET イメージング. 第 8 回日本分子イメージング学会総会･学術総会　2013 年 5 月 30 日　横浜
6. 原田龍一、岡村信行、古本祥三、多胡哲郎、吉川雄朗、荒井啓行、谷内一彦、工藤幸司. タウイメージング用トレーサー[^{18}F]THK-5117 の結合性評価. 第 8 回日本分子イメージング学会総会・学術総会　2013 年 5 月 30 日　横浜

G．知的財産権の出願・登録状況（予定も含む）

１．特許取得

特許出願状況を次および次々ページに示しました（すべて国内移行）。

２．実用新案登録

なし

３．その他

なし

特許出願状況

発明の名称	発明者	出願人	出願登録区分	出願番号（出願日）	出願区分	出願国	メモ
タウイメージングプローブ	工藤幸司 岡村信行 古本祥三	クリノ株式会社	出願	14102100.7（2014年3月3日）	国外	香港	国内移行
タウイメージングプローブ	工藤幸司 岡村信行 古本祥三	クリノ株式会社	出願	2013124812(2013年5月28日）	国外	ロシア	国内移行
タウイメージングプローブ	工藤幸司 岡村信行 古本祥三	クリノ株式会社	出願	2011321310（2013年4月21日）	国外	オーストラリア	国内移行
タウイメージングプローブ	工藤幸司 岡村信行 古本祥三	クリノ株式会社	出願	225888（2013年4月22日）	国外	イスラエル	国内移行
タウイメージングプローブ	工藤幸司 岡村信行 古本祥三	クリノ株式会社	出願	2013－7013588(2013年5月28日）	国外	韓国	国内移行
タウイメージングプローブ	工藤幸司 岡村信行 古本祥三	クリノ株式会社	出願	11836445.4(2013年5月23日）	国外	ヨーロッパ	国内移行
タウイメージングプローブ	工藤幸司 岡村信行 古本祥三	クリノ株式会社	出願	2815960(2013年4月25日)	国外	カナダ	国内移行
タウイメージングプローブ	工藤幸司 岡村信行 古本祥三	クリノ株式会社	出願	ＢＲ 112013010333-7（2013年4月26日）	国外	ブラジル	国内移行
タウイメージングプローブ	工藤幸司 岡村信行 古本祥三	クリノ株式会社	出願	201303398－0(2013年4月29日）	国外	シンガポール	国内移行
タウイメージングプローブ	工藤幸司 岡村信行 古本祥三	クリノ株式会社	出願	13/881872（2013年4月26日）	国外	アメリカ	国内移行
タウイメージングプローブ	工藤幸司 岡村信行 古本祥三	クリノ株式会社	出願	特願：2012-540957（2013年4月25日）	国内	日本	国内移行
タウイメージングプローブ	工藤幸司 岡村信行 古本祥三	クリノ株式会社	出願	201180062845.8（2013年6月16日）	国外	中国	国内移行

発明の名称	発明者	出願人	出願登録区分	出願番号（出願日）	出願区分	出願国	メモ
タウイメージングプローブ	工藤幸司 岡村信行 古本祥三	クリノ株式会社	出願	W 00201301795 （2013年4月26日）	国外	インドネシア	国内移行
タウイメージングプローブ	工藤幸司 岡村信行 古本祥三	クリノ株式会社	出願	MX/A2013/004834(2013年4月29日)	国外	メキシコ	国内移行
タウイメージングプローブ	工藤幸司 岡村信行 古本祥三	クリノ株式会社	出願	3985/CHENP/2013(2013年5月21日)	国外	インド	国内移行

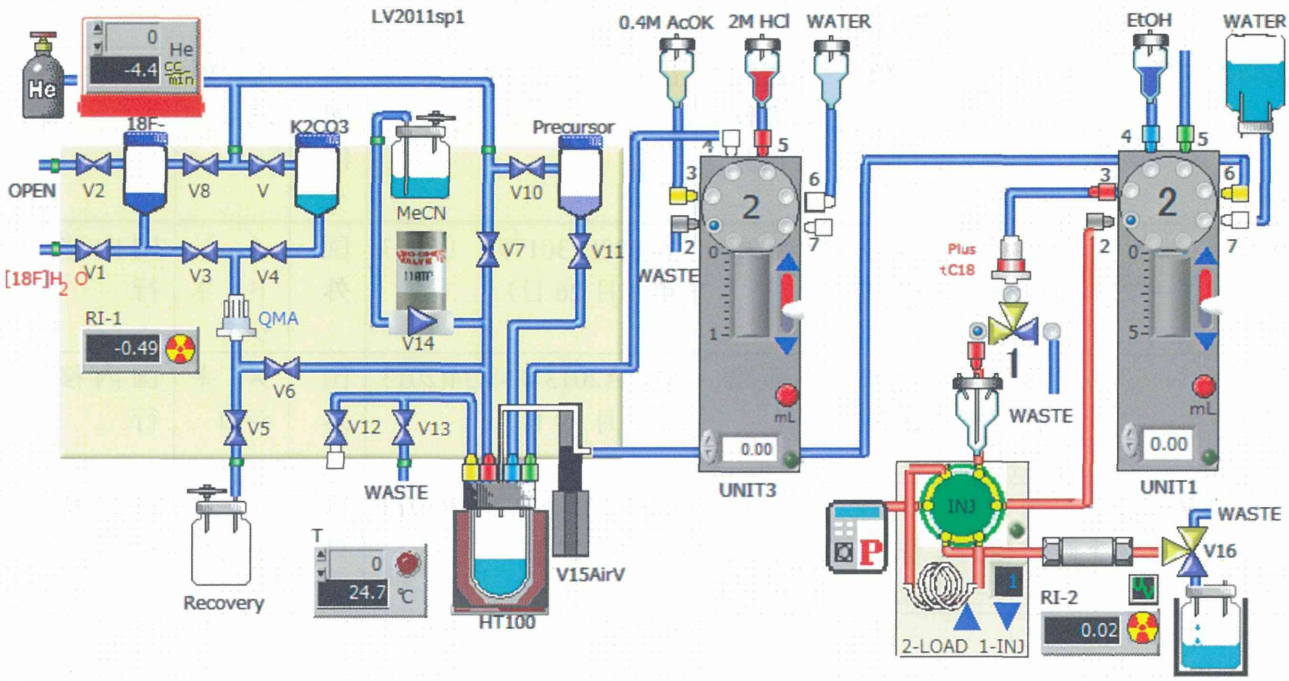

図１　標識合成装置の制御画面図。流路接続、電磁弁、温度モニター、流量モニター、放射能モニター、電動シリンジ、固相抽出ユニット、**HPLC** 送液システム、**HPLC** カラム、各種リザーバーなどが表示されている。

図２　標識合成後の固相抽出操作のモニター画像。黄色の脂溶性粗生成物が固相上に補足され、洗浄操作で流出することなく、その後の溶出操作で溶出していく様子が確認できる。

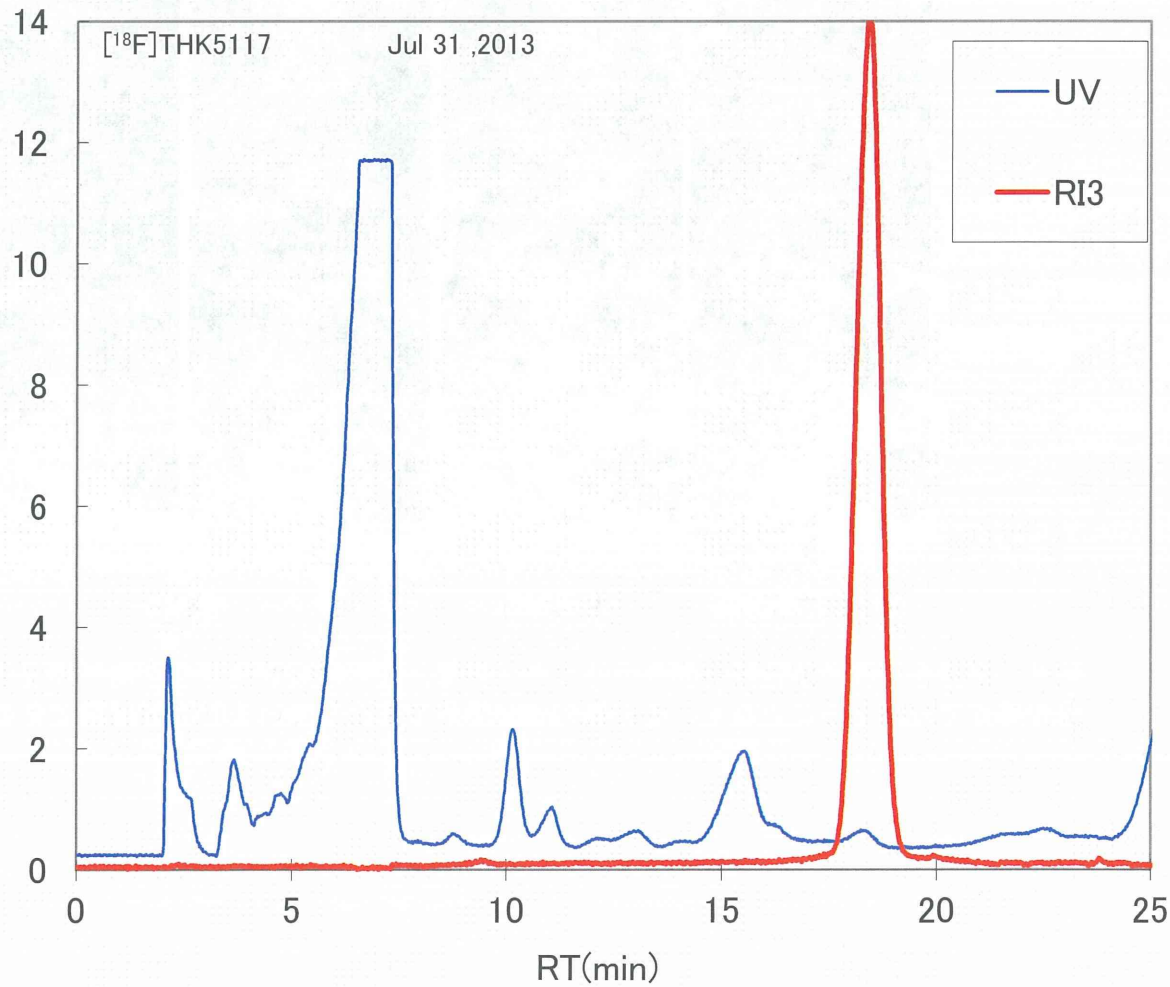

図３　セミ分取高速液体クロマトグラフィーで得られたクロマトグラムの典型例。青線は UV 吸収のクロマトグラムを表し、赤線は放射能のクロマトグラムを表している。UV クロマトグラムから明らかなように、目的とする THK5117 以外の非放射性夾雑物の混入は見られない。UV ピークサイズが小さいことは、製造された[^{18}F]THK5117 の比放射能が高いことを示している。

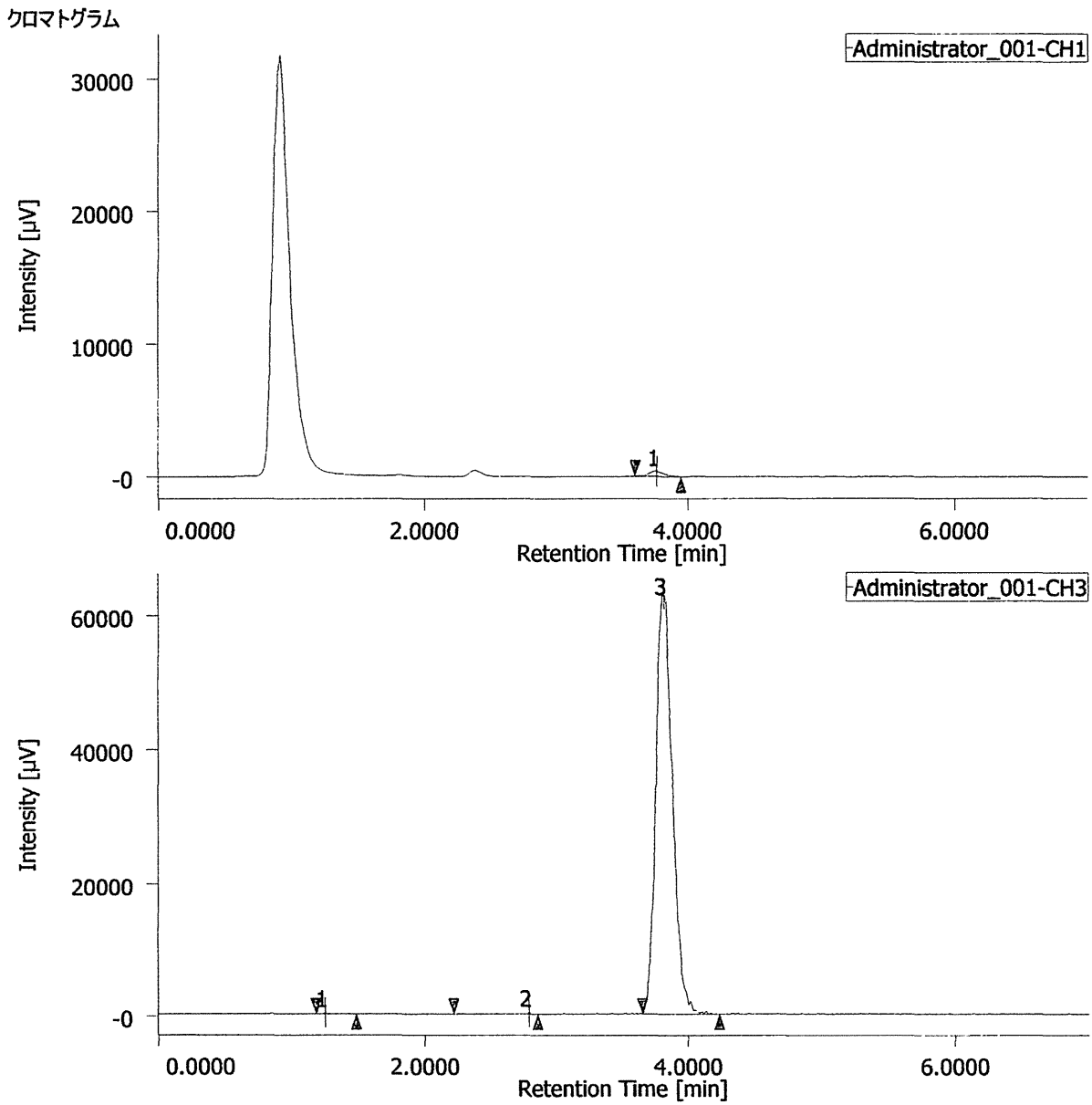

図４　分析高速液体クロマトグラフィーで得られた[^{18}F]THK5117 のクロマトグラム。上段は UV 吸収のクロマトグラムで、保持時間約 3.6 分のピーク 1 が THK5117 である。下段は放射線のクロマトグラムで、保持時間約 3.6 分のピーク 3 が[^{18}F]THK5117 である。[^{18}F]THK5117 以外の放射性ピークはほとんど観察されず、放射化学的純度は非常に高いことが分かる。

研究成果の刊行に関する一覧表

研究成果の刊行に関する一覧表

雑誌

下記「Brain. doi:10.1093/brain /awu064」の内容が「Nature Reviews Neurology. Doi:10.1038/nmeurol.2014.71」に紹介されました。

発表者氏名	論文タイトル名	発表誌名	巻号	ページ	出版年
Okamura N, Furumoto S, Fedoro-Tavoletti MT Mulligan RS, Harada R, Yates P, Pejoska S, Kudo Y, Masters CL, Yanai K. Rowe CC, Villemagne VL	Non-invasive assessment of Alzheimer's disease neurofibrillary pathology using 18F-THK-5105 PET	Brain doi:10.1093/brain /awu064	doi:10.1093/ brain /awu064		2014
Fodero-Tavoletti MT, Furumoto S, Taylor L, McLean CA, Mulligan RS, Birchall I,Harada R,Masters CL,Yanai K, Kudo Y,Rowe CC,Okamura N,Villemagne VL:	Assessing THK523 selectivity for tau deposits in Alzheimer's disease and non Alzheimer's disease tauopathies.	Alzheimers Res Ther 2611-19	26	11-19	2014
TagoT,Furumoto S,Okamura N,Harada R,Ishikawa Y,Arai H,Yanai K,Iwata R,Kudo Y.	Synthesis and preliminary evaluation of 2-arylhydroxyquinoline derivatives for tau imaging.	J Labelled Comp Radiophaem57(1)18-24	57	18-24	2014
VillemagneVL,Furumoto S,Fodero-Taboletti MT,Mulligan RS,Hodges J,Harada R,Yates P,Piguet O,Pejoska S,Dore V,Yanai K,MastersCL,KudoY,Rowe CC,Okamura N.	In vivo evaluation of a novel tau imaging tracer for Aizheimer's disease	Eur J Nucl Med Mol Imaging41.816-826	41	816-826	2014

Tomita N, Furukawa K, Okamura N, Tashiro M, Une K, Furumoto S, Iwata R, Yanai K, Kudo Y, Arai H	Brain accumulation of amyloid β protein visualized by positoron emission tomography and BF-227 in Alzheimer's disease patients with or without diabetes mellitus	Geriatr Gerontol Int. 13.215-221	13	215-221	2013
Harada R, Okamura N, Furumoto S, Tago T, Maruyama M, Higuchi M, YosikawaT, Arai H, Iwata R, Kudo Y, Yanai K	Comparison of the binding characteri stics of [(18)F]THK- 523 and other amyloid imaging tracers to Alzheimer's disease patholopgy	ur J Nucl Med Mol Imaging 40.125-132	40	125-132	2013
Furumoto S, Okamura N, Furukawa K, Tashiro M, Ishikawa Y, Sugi K, Tomita N, Waragai M, Harada R, Tago T, Iwata R, Yanai K, Arai H, Kudo Y	A (18)F-Labeled BF-227 Derivative as a Potential Radioligand for Imaging Dense Amyloid Plaques by Positron Emission Tomography	Mol Imaging Biol.15.497-506	15	497-506	2013
Shidahara M,Tashiro M,Okamura N,Furumoto S,Furukawa K,Watanuki S,Hiraoka K,Miyake M,Iwata R,Tamura H,Arai H,Kudo Y,Yanai K.	Evaluation of the biodistribution and radiation dosimetry of the 18F-labelled amyloid imaging probe [18F]FACT in humans.	EJNMMI Res.3.32-41	3	32-41	2013
Harada R,Okamura N,Furumoto S,Yoshikawa T, Arai H,Yanai K,Kudo Y.	Use of a Benzimidazole Derivative BF-188 in Fluorescence Multispectral Imaging for Selective Visualization of Tau Protein Fibrils in the Alzheimer's Disease Brain.	Mol Imaging Biol.16.19-27	16	19-27	2013

Maruyama.M, Shimada H, Suhara T, Shinotoh H,Bin J,Maeda J,M.R.Z, Trojanowski.J.Q,Lee V.M.Y, Ono M,Masamoto K,Takano H,Sahara N,Iwata N,Okamura N, Furumoto S, Kudo Y, Chang Q,Saido C.T,Takashima A,Jada L,M.K.J,Aoki I,Ito H,Higuchi M.	Imaging of Tau Pathology in a Ttauopathy Mouse Model and in Alzheimer Patients Compared to Normal Controls.	Neuron 79.1094 -1108	79	1094-1108	2013

研究成果の刊行に関する一覧表

書籍

著者氏名	論文タイトル名	書籍全体の編集者名	書籍名	出版社名	出版地	出版年	ページ
工藤幸司 荒井啓行	脳アミロイドーシス	田村和夫	血液症候群（第2版） 別冊 日本臨床	株式会社日本臨床社	大阪市	2013	648 -652

研究成果の刊行物・別刷

Brain Advance Access published March 27, 2014

doi:10.1093/brain/awu064 Brain 2014: Page 1 of 10 | 1

BRAIN
A JOURNAL OF NEUROLOGY

Non-invasive assessment of Alzheimer's disease neurofibrillary pathology using ^{18}F-THK5105 PET

Nobuyuki Okamura,[1] Shozo Furumoto,[2] Michelle T. Fodero-Tavoletti,[3,4] Rachel S. Mulligan,[4] Ryuichi Harada,[1] Paul Yates,[4] Svetlana Pejoska,[4] Yukitsuka Kudo,[5] Colin L. Masters,[3,6] Kazuhiko Yanai,[1,2] Christopher C. Rowe[4] and Victor L. Villemagne[3,4]

1 Department of Pharmacology, Tohoku University School of Medicine, Sendai, Japan
2 Cyclotron and Radioisotope Centre, Tohoku University, Sendai, Japan
3 The Florey Institute of Neuroscience and Mental Health, The University of Melbourne, Australia
4 Centre for PET, Austin Health, Melbourne, Australia
5 Clinical Research, Innovation and Education Centre, Tohoku University Hospital, Sendai, Japan
6 The Mental Health Research Institute, Melbourne, Australia

Correspondence to: Nobuyuki Okamura,
Department of Pharmacology,
Tohoku University School of Medicine,
2-1 Seiryo-machi, Aoba-ku,
Sendai, 9808575, Japan
E-mail: nookamura@med.tohoku.ac.jp

Non-invasive imaging of tau pathology in the living brain would be useful for accurately diagnosing Alzheimer's disease, tracking disease progression, and evaluating the treatment efficacy of disease-specific therapeutics. In this study, we evaluated the clinical usefulness of a novel tau-imaging positron emission tomography tracer ^{18}F-THK5105 in 16 human subjects including eight patients with Alzheimer's disease (three male and five females, 66–82 years) and eight healthy elderly controls (three male and five females, 63–76 years). All participants underwent neuropsychological examination and 3D magnetic resonance imaging, as well as both ^{18}F-THK5105 and ^{11}C-Pittsburgh compound B positron emission tomography scans. Standard uptake value ratios at 90–100 min and 40–70 min post-injection were calculated for ^{18}F-THK5105 and ^{11}C-Pittsburgh compound B, respectively, using the cerebellar cortex as the reference region. As a result, significantly higher ^{18}F-THK5105 retention was observed in the temporal, parietal, posterior cingulate, frontal and mesial temporal cortices of patients with Alzheimer's disease compared with healthy control subjects. In patients with Alzheimer's disease, the inferior temporal cortex, which is an area known to contain high densities of neurofibrillary tangles in the Alzheimer's disease brain, showed prominent ^{18}F-THK5105 retention. Compared with high frequency (100%) of ^{18}F-THK5105 retention in the temporal cortex of patients with Alzheimer's disease, frontal ^{18}F-THK5105 retention was less frequent (37.5%) and was only observed in cases with moderate-to-severe Alzheimer's disease. In contrast, ^{11}C-Pittsburgh compound B retention was highest in the posterior cingulate cortex, followed by the ventrolateral prefrontal, anterior cingulate, and superior temporal cortices, and did not correlate with ^{18}F-THK5105 retention in the neocortex. In healthy control subjects, ^{18}F-THK5105 retention was ~10% higher in the mesial temporal cortex than in the neocortex. Notably, unlike ^{11}C-Pittsburgh compound B, ^{18}F-THK5105 retention was significantly correlated with cognitive parameters, hippocampal and whole brain grey matter volumes, which was consistent with findings from previous post-mortem studies showing significant correlations of neurofibrillary tangle density with dementia severity or neuronal loss. From these results, ^{18}F-THK5105 positron emission tomography is considered to be useful for the non-invasive assessment of tau pathology in the living brain. This technique would be applicable to the longitudinal evaluation of tau deposition and allow a better understanding of the pathophysiology of Alzheimer's disease.

Received December 11, 2013. Revised January 12, 2014. Accepted February 4, 2014.

Keywords: Alzheimer's disease; Alzheimer's disease pathology; amyloid; positron emission tomography; PET

Abbreviations: CDR = *clinical dementia rating*; MMSE = *Mini-Mental State Examination*; PiB = *Pittsburgh compound* B; SOB = *sum* of boxes; SUV = standardized uptake value; SUVR = ratio of regional SUV to cerebellar cortex SUV ratio

Introduction

Senile plaques and neurofibrillary tangles are considered the major pathological hallmarks of Alzheimer's disease (Braak and Braak, 1991). Senile plaques consist of extracellular aggregates of amyloid-β peptide cleaved from a longer amyloid precursor protein (Masters *et al.*, 2006). The neocortical deposition of senile plaques is considered one of the earliest pathological alterations in Alzheimer's disease and is observed even in the presymptomatic stages (Mintun *et al.*, 2006; Rowe *et al.*, 2007; Price *et al.*, 2009). Recently proposed research diagnostic criteria for preclinical Alzheimer's disease include cognitively intact elderly with abnormal amyloid-β deposition in the brain (Sperling *et al.*, 2011). Preclinical Alzheimer's disease is associated with future cognitive decline and mortality (Vos *et al.*, 2013); however, several neuropathological studies have shown no significant association between density of amyloid-β plaques and the severity of dementia or neuronal loss (Arriagada *et al.*, 1992; Bierer *et al.*, 1995; Gomez-Isla *et al.*, 1997), suggesting the involvement of other key factors in Alzheimer's disease-related neurodegeneration.

Neurofibrillary tangles are comprised of paired helical filaments that result from the abnormal aggregation of tau protein (Grundke-Iqbal *et al.*, 1986*a*, *b*; Lee *et al.*, 1991). Initial neurofibrillary tangle lesions occur in the trans-entorhinal cortex, followed by entorhinal cortex and hippocampus involvement, progressing to temporal neocortex and finally to the other neocortical areas (Arnold *et al.*, 1991; Braak and Braak, 1991). In contrast with senile plaques, neurofibrillary tangle formation correlates well with cognitive impairment severity (Arriagada *et al.*, 1992; Berg *et al.*, 1993; Bierer *et al.*, 1995), an association that is considered to continue throughout the disease course (Abner *et al.*, 2011). Furthermore, the inhibition of abnormal tau hyperphosphorylation and its aggregation appear to be promising therapeutic strategies in Alzheimer's disease. Thus, non-invasive imaging of tau pathology would be useful to assist in the early and differential diagnosis of dementia, track the progression of disease-related pathology, and monitor the efficacy of anti-tau treatments.

^{18}F-FDDNP has been reported to detect neurofibrillary tangle deposition (Shoghi-Jadid *et al.*, 2002) and successfully differentiate subjects with Alzheimer's disease and mild cognitive impairment from those with no cognitive impairment (Small *et al.*, 2006). However, this tracer detects the combined signals of senile plaques and neurofibrillary tangles (Shoghi-Jadid *et al.*, 2002). Several radiotracers have been developed for the selective visualization of neurofibrillary tangles in the living brain (Chien *et al.*, 2013, 2014; Maruyama *et al.*, 2013). Early clinical PET studies successfully differentiated patients with Alzheimer's disease from cognitively normal elderly. However, the selective binding ability of these radiotracers to tau has not been fully validated *in vivo*.

For the development of a selective tau radiotracer, we screened β-sheet-binding small molecules and identified novel quinoline derivatives with high binding selectivity to tau deposits in Alzheimer's disease brain samples (Okamura *et al.*, 2005; Fodero-Tavoletti *et al.*, 2011; Harada *et al.*, 2013). Through a compound optimization process, we developed a novel ^{18}F-labelled 2-arylquinoline derivative, ^{18}F-THK5105 (Fig. 1), which showed high binding affinity and selectivity to tau protein deposits in Alzheimer's disease brain sections (Okamura *et al.*, 2013). This ^{18}F-labelled radiotracer also exhibited high blood–brain barrier permeability and no defluorination in mice (Okamura *et al.*, 2013). The present clinical study evaluated whether ^{18}F-THK5105 PET could selectively bind to tau pathology in living patients with Alzheimer's disease.

Materials and methods

Participants

Sixteen subjects, including eight patients with probable Alzheimer's disease (three male and five females, age range 66–82 years) and eight age-matched healthy control subjects (three male and five females, age range 63–76 years), underwent both ^{18}F-THK5105 and ^{11}C-labelled Pittsburgh compound B (^{11}C-PiB) PET scans (Table 1). Written informed consent was obtained from all participants. Study approval was obtained from the Austin Health Human Research Ethics Committee. Elderly healthy controls were recruited by advertisements in the community, and patients with Alzheimer's disease were recruited from tertiary Memory Disorders Clinics or physicians who sub-specialize in dementia care. All participants were reviewed and classified on the basis of their clinical and neuropsychological performance by the consensus of a neurologist and a neuropsychologist who were blind to their PET results. The diagnosis of Alzheimer's disease was made according to the National Institute of Neurological and Communicative Disorders and Stroke/Alzheimer's Disease and Related Disorders Association (NINCDS-ADRDA) criteria.

Neuropsychological evaluation

Cognitive impairment and dementia severity were evaluated with the Mini-Mental State Examination (MMSE), the Clinical Dementia Rating (CDR) and the CDR scale sum of boxes (CDR-SOB). In addition, composite episodic memory and non-memory scores were generated as previously described (Villemagne *et al.*, 2011). Briefly, a composite episodic memory score was calculated by taking the average of the *z*-scores for the Rey Complex Figure Test, the long delay California Verbal Learning Test, Second Edition, and the Logical Memory II subscale of the Wechsler Memory Scale. A composite non-memory score was calculated by taking the average of the *z*-scores for the Boston Naming Test, letter fluency, category fluency, digit span forwards and backwards, digit symbol-coding, and Rey Complex Figure Test copy.

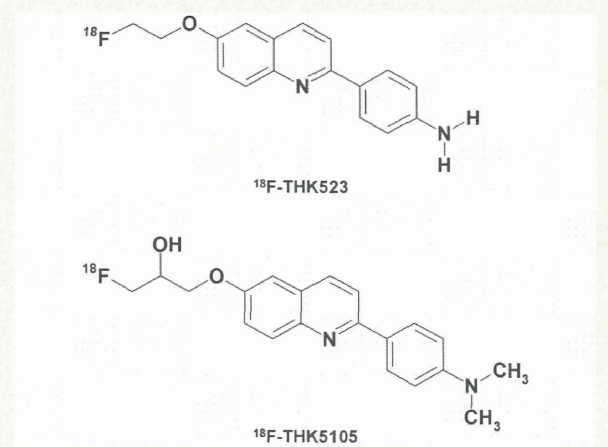

Figure 1 Chemical structures of ^{18}F-THK523 and ^{18}F-THK5105.

Table 1 Demographic characteristics of healthy control and Alzheimer's disease subjects

	Healthy controls ($n = 8$)	Alzheimer's disease ($n = 8$)
Age	70.5 ± 4.4	74.1 ± 6.9
Gender (M/F)	3/5	3/5
Years of education	15.4 ± 2.4	11.3 ± 3.2*
CDR	0.0	0.9 ± 0.5*
CDR-SOB	0.0	6.1 ± 4.9*
MMSE score	28.8 ± 1.5	17.3 ± 6.6*
Episodic memory scores	−0.1 ± 0.8	−3.8 ± 0.3*
Non-memory scores	−0.1 ± 0.5	−3.0 ± 1.9*
Grey matter volume (cm^3)	302.7 ± 12.9	272.9 ± 22.6*
Hippocampal volume (cm^3)	4.8 ± 0.5	4.0 ± 0.6*

*$P < 0.05$ by the Mann–Whitney U test.

Image acquisition

MRI scanning was performed on a 3 T Siemens TRIO magnetic resonance system (Siemens Healthcare) using the ADNI 3D MPRAGE sequence with 1 × 1 mm in-plane resolution and 1.2 mm slice thickness, repetition time/echo time/inversion time = 2300/2.98/900, flip angle 9°, field of view 240 × 256, and 160 slices. T_2 fast spin echo and FLAIR sequences were also obtained.

Two radiotracers, ^{18}F-THK5105 and ^{11}C-PiB, were prepared in the Centre for PET at Austin Hospital. ^{18}F-THK5105 was synthesized by nucleophilic substitution of the tosylate precursor as described previously (Okamura *et al.*, 2013). The decay-corrected average radiochemical yield of the production of ^{18}F-THK5105 was 45%, with a radiochemical purity >95% and a specific activity of 229.6 GBq/μmol (6.2 ± 3.3 Ci/μmol). ^{11}C-PiB was synthesized using the one-step ^{11}C-methyl triflate approach as previously described (Rowe *et al.*, 2007). The decay-corrected average radiochemical yield for ^{11}C-PiB was 30%, with a radiochemical purity >98% and a specific activity of 30 ± 7.5 GBq/μmol.

A list-mode emission acquisition on an Allegro™ PET camera (Philips Medical Systems) was performed in 3D mode from 0–50 min and between 90–120 min after injection of 200 MBq ^{18}F-THK5105. List-mode raw data for the initial 50 min of the acquisition were sorted off-line into 6 × 30-s, 7 × 1-min, 4 × 2.5-min, 2 × 5-min, and 6 × 10-min frames. The final 30 min were acquired as 6 × 5-min frames. The sorted sinograms were reconstructed using a 3D RAMLA algorithm. A 30-min acquisition (6 × 5-min frames) on an Allegro™ PET camera began 40 min after intravenous injection of 300 MBq ^{11}C-PiB.

Image analysis

Hippocampal and cortical grey matter volumes were obtained using an automated volumetric measurement program (NeuroQuant: CorTechs Labs Inc) applied to the 3D MP RAGE MRI images. The primary MRI outcome measures were the grey cortical matter and hippocampal volumes normalized to total intracranial volume.

PET images were processed using a semi-automatic region of interest method. Firstly, standardized uptake value (SUV) images of ^{18}F-THK5105 and ^{11}C-PiB were obtained by normalizing tissue radioactivity concentration by injected dose and body weight. Subsequently, individual MRI T_1 images were anatomically co-registered into individual PET images using Statistical Parametric Mapping software (SPM8: Wellcome Trust Centre for Neuroimaging, London, UK). Co-registered MRI and PET images were then spatially normalized to an MRI T_1 template in Talairach space using SPM8. After spatial normalization, a region of interest template was placed on individual axial images in the cerebellar hemisphere, ventrolateral frontal cortex [Brodmann areas (BA) 10, 44, 45 and 46], lateral and medial orbitofrontal cortex (BA 11 and 12), superior temporal cortex (BA 22), inferior temporal cortex (BA 20 and 37), parietal cortex (BA 39 and 40), lateral occipital cortex (BA 18 and 19), anterior cingulate cortex, posterior cingulate cortex, mesial temporal cortex (BA 27, 28, 34 and 35), putamen, pons, and subcortical white matter. Regional SUVs were sampled using PMOD software (PMOD Technologies, Ltd).The ratio of regional SUV to cerebellar cortex SUV ratio (SUVR) was used as an index of tracer retention. Neocortical tau and amyloid-β burden were expressed as the average SUVR for the following cortical regions of interest: frontal, parietal, lateral temporal, and posterior cingulate for THK5105 and PiB, respectively. As in previous studies, a PiB SUVR threshold of 1.5 was used to categorize high and low amyloid-β burden.

Statistical analysis

Mann-Whitney's U-tests were applied for comparison of the Alzheimer's disease and healthy control groups. For comparison of regional radiotracer uptake, one-way repeated measures analysis of variance (ANOVA) followed by Bonferroni's tests were performed. To examine the regional difference of tracer retention between neocortex and mesial temporal cortex, Wilcoxon matched-pairs signed rank tests were performed. Effect size coefficients (Cohen's d) were calculated for the evaluation of group differences in PET measurements. Statistical significance for each analysis was defined as $P < 0.05$. Data are presented as mean ± standard deviation (SD).

Results

Healthy control and Alzheimer's disease subject demographics are shown in Table 1. There were no significant differences between healthy control and Alzheimer's disease groups with regard to age

or gender; however, the Alzheimer's disease group was significantly less educated than the healthy control group. As expected, significant differences between the two groups were observed for CDR and CDR-SOB scores, cognitive performance (MMSE, episodic memory, and non-memory scores), and brain volumetrics (grey matter and hippocampal volumes).

No toxic event was observed in the current clinical PET study. After intravenous administration of ^{18}F-THK5105, all subjects showed rapid entry of the tracer into grey matter areas. The SUV time activity curves of ^{18}F-THK5105 PET are shown in Fig. 2. The peak uptake and clearance rates of ^{18}F-THK5105 in the cerebellar cortex were similar between healthy control (Fig. 2A) and Alzheimer's disease (Fig. 2B) groups. In patients with Alzheimer's disease, the inferior temporal cortex, which is an area known to contain high densities of neurofibrillary tangles in Alzheimer's disease (Bouras *et al.*, 1994), showed ^{18}F-THK5105 retention compared to the cerebellum, especially at the later time points. In contrast, time activity curves in the inferior temporal cortex of healthy control subjects were nearly identical to those in the cerebellum. The subcortical white matter region showed relatively lower entry and slower clearance than grey matter areas, but no significant differences were observed for time activity curves between healthy control and Alzheimer's disease groups (data not shown). The ratio of inferior temporal cortex to cerebellar SUVR became constant in all participants ~90 min after injection of ^{18}F-THK5105 (Fig. 2C). Therefore, we selected SUVR values from 90–100 min post-injection for the following analysis.

Summed SUVR images from 90–100 min post-injection for healthy control and Alzheimer's disease subjects are shown in Fig. 3. Contrasted with a lack of remarkable ^{18}F-THK5105 retention in the grey matter of healthy control subjects, patients with Alzheimer's disease showed high grey matter ^{18}F-THK5105 retention in the lateral and mesial temporal regions. ^{18}F-THK5105 retention was additionally observed in the brain stem; however, similar retention in these areas was detected in healthy control subjects. When comparing the 90–100 min regional SUVR in Alzheimer's disease and healthy control subjects, ^{18}F-THK5105 SUVRs for the ventrolateral prefrontal, medial orbitofrontal, superior, and inferior temporal, parietal, posterior cingulate, and mesial temporal cortices were significantly higher in patients with Alzheimer's disease (Table 2 and Fig. 4). Notably, SUVR in the inferior temporal cortex showed no overlap between the Alzheimer's disease and healthy control groups (Fig. 4). ^{18}F-THK5105 retention in other neocortical areas was relatively lower than in the inferior temporal area. The SUVR in the parietal cortex was elevated in 62.5% (5/8) of patients with Alzheimer's disease; however, ^{18}F-THK5105 retention in the ventrolateral prefrontal cortex was only elevated in 37.5% (3/8) of patients with Alzheimer's disease. Mesial temporal ^{18}F-THK5105 retention was significantly higher in patients with Alzheimer's disease than in healthy control subjects. However, a substantial overlap of SUVR was observed between both groups. The SUVR values in the pons and subcortical white matter were nearly identical in both groups, but higher than other neocortical regions. The effect size value between Alzheimer's disease and healthy control subjects was highest in the inferior temporal cortex, followed by the superior temporal, posterior cingulate, parietal, and medial orbitofrontal cortices and was lowest in the other regions examined (Table 2). Regional difference of ^{18}F-THK5105 retention was additionally examined in healthy control subjects. As a result, mesial temporal ^{18}F-THK5105 retention (mean SUVR = 1.17) was significantly higher than neocortical ^{18}F-THK5105 retention (mean SUVR = 1.05) in healthy control subjects.

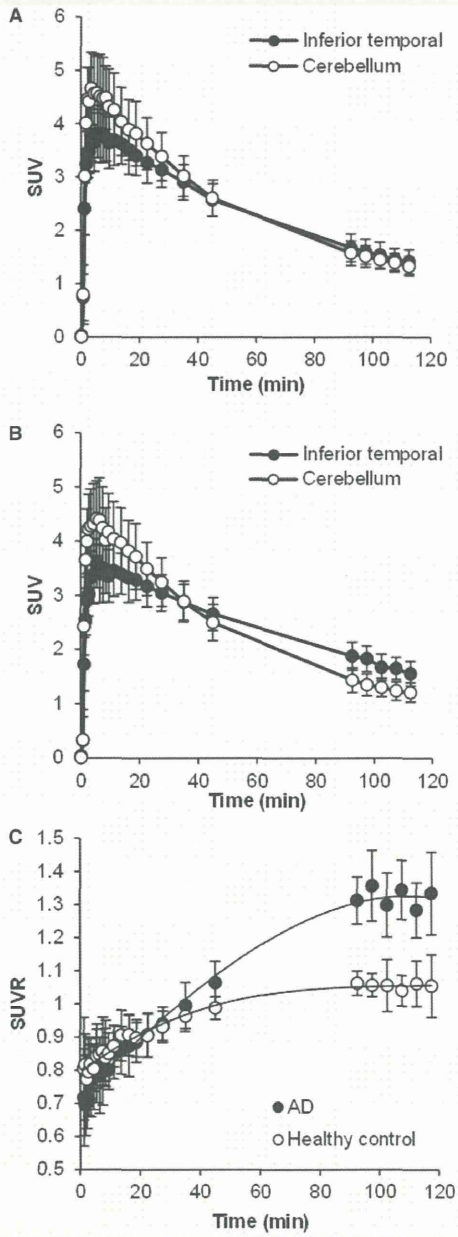

Figure 2 (**A** and **B**) ^{18}F-THK5105 SUV TACs in the cerebellum (open circles) and inferior temporal cortex (filled circles) of eight healthy control subjects (**A**) and eight patients with Alzheimer's disease (**B**). (**C**) SUVR time activity curves of ^{18}F-THK5105 PET in eight healthy control subjects (open circles) and eight patients with Alzheimer's disease (AD) (filled circles). Each point represents the mean ± SD.

As reported in previous PET studies (Klunk *et al.*, 2004; Mintun *et al.*, 2006; Rowe *et al.*, 2007), ^{11}C-PiB SUVR values were significantly greater in the neocortical regions of patients with Alzheimer's disease compared to healthy control subjects (Table 3). All patients with Alzheimer's disease showed marked and extensive PiB retention in neocortical areas. On the other hand, neocortical PiB retention in healthy control subjects was not significant, except for one healthy control case that only showed high ^{11}C-PiB retention in the frontal cortex. In contrast

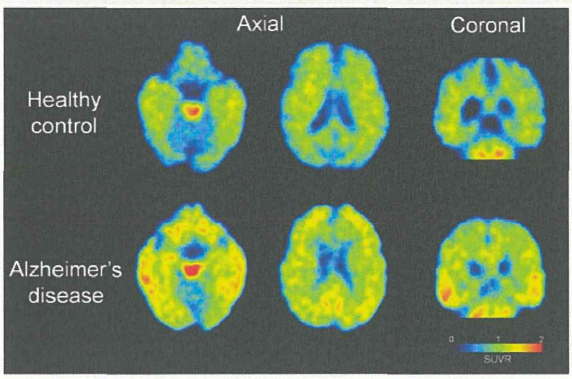

Figure 3 ^{18}F-THK5105 PET images from 60–80 min post-injection in a healthy control subject (72-years-old, CDR 0, MMSE 29) and a patient with Alzheimer's disease (68-years-old, CDR 1.0, MMSE 20).

Table 2 Regional ^{18}F-THK5105 SUVR values in healthy control and Alzheimer's disease subjects

Region	Healthy controls	Alzheimer's disease	Cohen's d
Ventrolateral prefrontal	1.08 ± 0.08	1.23 ± 0.14*	1.33
Lateral orbitofrontal	1.01 ± 0.08	1.15 ± 0.13	1.32
Medial orbitofrontal	1.17 ± 0.06	1.29 ± 0.09*	1.55
Superior temporal	1.04 ± 0.06	1.22 ± 0.07*	2.75
Inferior temporal	1.09 ± 0.04	1.32 ± 0.08*	3.58
Parietal	0.99 ± 0.08	1.16 ± 0.13*	1.59
Lateral occipital	1.07 ± 0.06	1.18 ± 0.15	1.01
Anterior cingulate	1.07 ± 0.11	1.12 ± 0.13	0.35
Posterior cingulate	1.04 ± 0.08	1.20 ± 0.12*	1.61
Mesial temporal	1.17 ± 0.05	1.26 ± 0.10*	1.17
Putamen	1.41 ± 0.10	1.52 ± 0.17	0.83
Pons	1.88 ± 0.14	1.89 ± 0.23	0.03
Subcortical white matter	1.22 ± 0.15	1.22 ± 0.15	0.01
Neocortex	1.05 ± 0.05	1.23 ± 0.08*	2.68

*$P < 0.05$ by the Mann–Whitney U test.

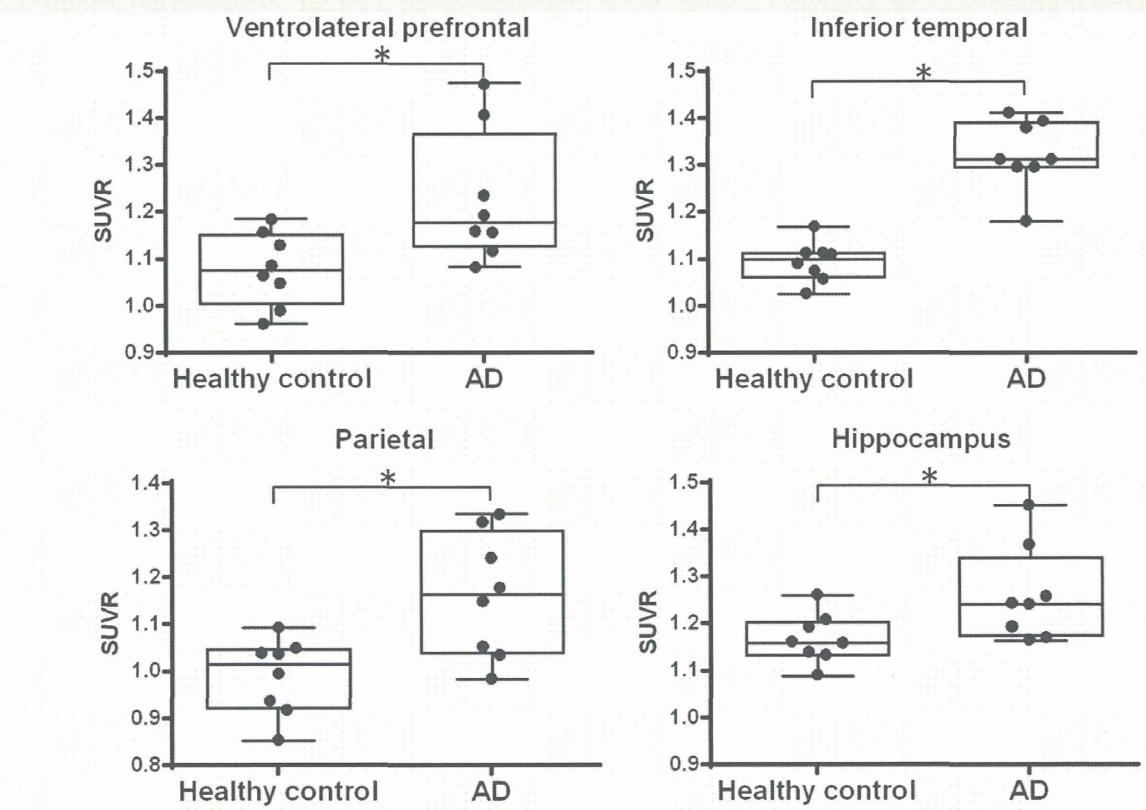

Figure 4 Regional ^{18}F-THK5105 SUVR values from 60–80 min post-injection in healthy control and Alzheimer's disease (AD) subjects. *$P < 0.05$ by the Mann–Whitney U test.

Table 3 Regional ^{11}C-PiB SUVR values in healthy control and Alzheimer's disease subjects

Region	Healthy controls	Alzheimer's disease	Cohen's d
Ventrolateral prefrontal	1.32 ± 0.39	2.92 ± 0.82*	2.49
Lateral orbitofrontal	1.08 ± 0.25	1.66 ± 0.50*	1.46
Medial orbitofrontal	1.36 ± 0.23	2.38 ± 0.63*	2.15
Superior temporal	1.11 ± 0.13	2.67 ± 0.67*	3.22
Inferior temporal	1.08 ± 0.08	2.42 ± 0.66*	2.88
Parietal	1.22 ± 0.17	2.56 ± 0.51*	3.54
Lateral occipital	1.25 ± 0.11	2.07 ± 0.61*	1.86
Anterior cingulate	1.39 ± 0.28	2.79 ± 0.70*	2.64
Posterior cingulate	1.31 ± 0.24	3.15 ± 0.78*	3.22
Mesial temporal	1.29 ± 0.15	1.65 ± 0.32*	1.42
Putamen	1.48 ± 0.20	2.64 ± 0.62*	2.50
Pons	2.04 ± 0.33	2.04 ± 0.40	0.00
Subcortical white matter	2.02 ± 0.38	2.06 ± 0.66	0.07
Neocortex	1.21 ± 0.14	2.75 ± 0.66*	3.21

*$P < 0.05$ by the Mann–Whitney U test.

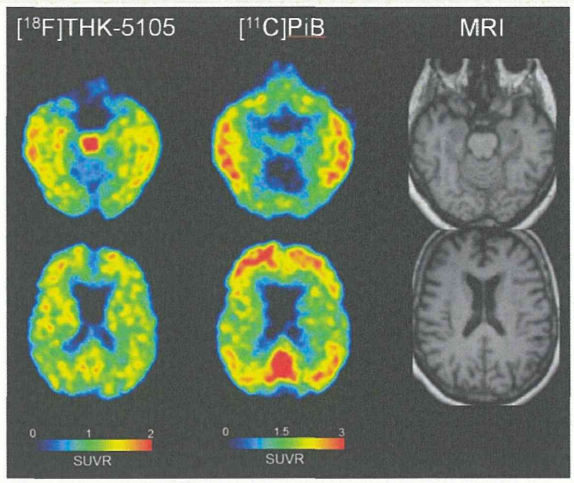

Figure 5 ^{18}F-THK5105 PET images from 60–80 min post-injection and ^{11}C-PiB PET images from 40–70 min post-injection in an Alzheimer's disease patient (68-years-old, CDR 1.0, MMSE 20). Co-registered magnetic resonance images are shown on the right.

with the highest neocortical ^{18}F-THK5105 retention in the inferior temporal cortex of patients with Alzheimer's disease, ^{11}C-PiB retention in the same group was highest in the posterior cingulate cortex, followed by the ventrolateral prefrontal, anterior cingulate, and superior temporal cortices. The PiB effect size value between Alzheimer's disease and healthy control subjects was also highest in the parietal cortex, followed by the posterior cingulate and superior temporal cortices. As shown in Fig. 5, the pattern of cortical ^{18}F-THK5105 retention was completely different from that of ^{11}C-PiB retention in patients with Alzheimer's disease, which was prominent in the frontal cortex and precuneus, but not evident in the mesial temporal cortex. In contrast, ^{18}F-THK5105 retention was evident in both lateral and mesial temporal areas but not so remarkable in other neocortical areas. There was no correlation between neocortical ^{18}F-THK5105 and ^{11}C-PiB SUVR values in patients with Alzheimer's disease ($r = 0.17$, $P = 0.703$). In addition, one healthy control case showing elevated PiB retention in the frontal cortex did not show any significant retention of ^{18}F-THK5105.

Finally, we explored the relationship of neocortical or mesial temporal radiotracer retention to cognitive parameters in patients with Alzheimer's disease. Neocortical ^{18}F-THK5105 retention was significantly correlated with MMSE scores ($r = -0.781$, $P = 0.022$), CDR ($r = 0.730$, $P = 0.050$) and CDR-SOB ($r = 0.779$, $P = 0.030$), but not correlated with composite episodic memory and non-memory scores. In contrast, neocortical ^{11}C-PiB retention showed no significant correlation with any cognitive parameters (Fig. 6). There was no correlation between radiotracer retention in mesial temporal cortex and cognitive parameters. Furthermore, we explored the relationship of radiotracer retention with brain volumetrics. When all subjects were included in the analysis, a significant correlation was observed between mesial temporal ^{18}F-THK5105 retention and hippocampal volumes ($r = -0.565$, $P = 0.023$) and between neocortical ^{18}F-THK5105 retention and whole brain grey matter volumes ($r = -0.649$, $P = 0.007$). When only patients with Alzheimer's disease were included in this analysis, hippocampal volumes were significantly correlated with neocortical ^{18}F-THK5105 retention ($r = -0.765$, $P = 0.027$), but not correlated with mesial temporal ^{18}F-THK5105 retention. However, there were no correlations between mesial temporal ^{11}C-PiB retention and hippocampal volumes and between neocortical ^{11}C-PiB retention and whole brain grey matter volumes (Fig. 7).

Discussion

In this study, the novel radiotracer ^{18}F-THK5105 successfully differentiated patients with Alzheimer's disease from healthy control subjects. The pattern of ^{18}F-THK5105 distribution in patients with Alzheimer's disease appears similar to the reported neurofibrillary tangle distribution in the post-mortem Alzheimer's disease brain. ^{18}F-THK5105 retention in the inferior temporal cortex, where neurofibrillary tangle accumulation is highest in Alzheimer's disease, was observed in most patients with Alzheimer's disease. In contrast to the high frequency of ^{18}F-THK5105 retention in the temporal cortices of Alzheimer's disease cases, ventrolateral prefrontal ^{18}F-THK5105 retention was less frequent (3/8) and was only observed in cases with moderate-to-severe Alzheimer's disease (MMSE range 10–17). This finding is consistent with neurofibrillary tangle distribution in post-mortem Alzheimer's disease brain, where there is a higher frequency of neurofibrillary tangles in the temporal cortex than the frontal cortex (Arnold *et al.*, 1991; Bouras *et al.*, 1994; Haroutunian *et al.*, 1999). It is also in agreement with recent PET results using other novel radiotracers (^{18}F-T807 and ^{18}F-T808) that demonstrated higher radiotracer retention in the lateral temporal lobe compared to the frontal lobe and selective binding ability to paired helical filament tau (Chien *et al.*, 2013, 2014). These findings suggest a spreading

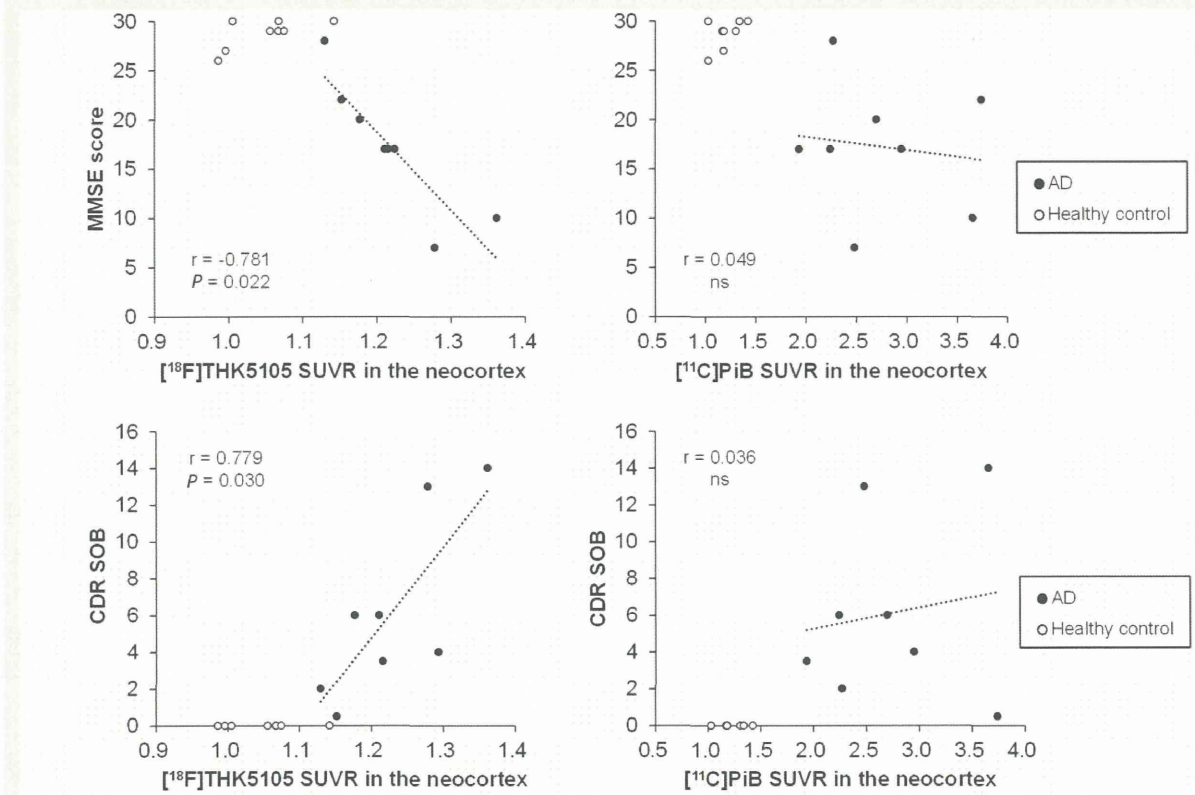

Figure 6 Correlation of neocortical ^{18}F-THK5105 and ^{11}C-PiB SUVR with MMSE scores (*upper*) and CDR-SOB scores (*lower*). Data from eight healthy control subjects (open circles) and eight patients with Alzheimer's disease (AD, filled circles) are shown.

of tau pathology (Soto, 2012; Mohamed *et al.*, 2013) from temporal areas to the other association cortices. A longitudinal assessment of tau pathology will help elucidate the spatial patterns of tau pathology progression in the living brain. In addition, as observed in ^{18}F-T807 and ^{18}F-T808 PET studies (Chien *et al.*, 2013, 2014), ^{18}F-THK5105 retention in the mesial temporal area was relatively lower than in the lateral temporal area in patients with Alzheimer's disease, which conflicts with microscopic observations showing higher neurofibrillary tangle density in the entorhinal cortex and hippocampus of Alzheimer's disease brain compared to the neocortex (Arnold *et al.*, 1991). One possible explanation for this phenomenon is the partial volume effect of radiotracer signals (Muller-Gartner *et al.*, 1992). ^{18}F-THK5105 retention in the mesial temporal cortex might be underestimated in patients with severe hippocampal atrophy.

^{18}F-THK5105 retention in patients with Alzheimer's disease was closely associated with dementia severity. This finding is consistent with results from previous post-mortem studies showing significant correlations of neurofibrillary tangle density with dementia severity (Arriagada *et al.*, 1992; Bierer *et al.*, 1995; Berg *et al.*, 1998). Our results further demonstrate that hippocampal atrophy is significantly correlated with ^{18}F-THK5105 retention but not with ^{11}C-PiB retention in the same area. In addition, the neocortical grey matter volume was negatively correlated with global ^{18}F-THK5105 retention in the neocortex. These findings correspond with the neuropathological observation that the density of neurofibrillary tangles, but not senile plaques, is closely associated with neuronal loss (Gomez-Isla *et al.*, 1996, 1997). Intriguingly, ^{18}F-THK5105 retention in healthy control subjects was significantly higher in the mesial temporal cortex (SUVR = 1.17) than in the neocortex (SUVR = 1.05). This finding is likely to reflect age-related tau accumulation in this area. In future studies, the association of mesial temporal ^{18}F-THK5105 retention with ageing should be evaluated in a large population. It is also still unclear whether or not tau accumulation precedes neuronal loss. To answer this question, mesial temporal cortex tau density should be evaluated in the mild cognitive impairment population, as well as cognitively normal individuals with amyloid-β deposition, and these results should be compared with fluorodeoxyglucose and brain atrophy in a longitudinal analysis.

The amount of neocortical ^{18}F-THK5105 retention (SUVR = 1.23) was considerably lower than that of ^{11}C-PiB (SUVR = 2.75) in patients with Alzheimer's disease. This is thought to result from higher concentrations of amyloid-β fibrils than tau fibrils in the Alzheimer's disease brain (Villemagne *et al.*, 2012). Therefore, a tau-specific radiotracer must be highly sensitive and selective to tau protein fibrils. Our previous study demonstrated that the binding affinity of ^{18}F-THK5105 for tau fibrils (Kd = 1.45 nM) was 25-times higher than to amyloid-β fibrils (Kd = 35.9 nM) (Okamura *et al.*, 2013). Autoradiography studies